Magnetic Designs of New First Target Beamline Magnets for the ORNL SNS Upgrade

V. Kashikhin, J. Amann, N. Evans, D. Harding, J. Holmes, M. Plum, D. Pomella

Abstract—**The Spallation Neutron Source (SNS) at ORNL currently is being upgraded from 1.0 GeV to 1.3 GeV. A number of water-cooled magnets should be upgraded to transport 30% of higher beam energy. New chicane, injection/extraction septum, and Lambertson magnets were designed. Designing the magnets was a challenging task because the new magnets required good combined integrated field quality and needed to occupy the old magnets space but with about 20% greater integrated magnetic field. Additional strong requirements applied to the magnets fringe field do not disturb the circulating beam. The special field profiles had to be provided in foil areas between magnets. The analysis described here was based on OPERA3D simulations. A special technique was used for analyzing the integrated field harmonics. Initially, the particle track was simulated, and integrated field components were calculated along this track for the reference radius, which were used for the harmonics analysis. In addition, 3D field maps were provided for beam optics simulations. The final beamline analysis confirmed good beam transmission and low losses.**

Index Terms—**Magnetic designs, Chicane magnets, Septum magnet, Lambertson magnet, OPERA3D simulations, harmonic analysis.**

I. INTRODUCTION

FOR the Spallation Neutron Source (SNS) [1], new magnets were designed for the beamline to the first target station because of an accelerator upgrade [2] from 1 GeV to 1.3 GeV particle energy. The old magnets were designed and built at BNL [3] – [6]. They successfully operated for many years but had to be replaced because about a 20% magnetic field increase was needed. The new magnets had to occupy the same slot space in the beamline as the old ones, which was a challenging task. Various additional requirements and limitations exist, including regarding the magnetic field around the foil, fringe fields in the injected beam areas, and field quality, which are reflected in the magnets' specifications. It was not enough during the magnets' design just to analyze the magnetic field quality without beam tracking. The OPERA simulation software [7] can combine magnetic field analysis with particle tracking to ensure more realistic field analysis of and designs for the beam path areas.

II. CHICANE MAGNETS

Two chicane magnets – D2 and D3, as shown in Fig. 1 were needed to provide the 50.1 mrad beam, bending in the horizontal plane.
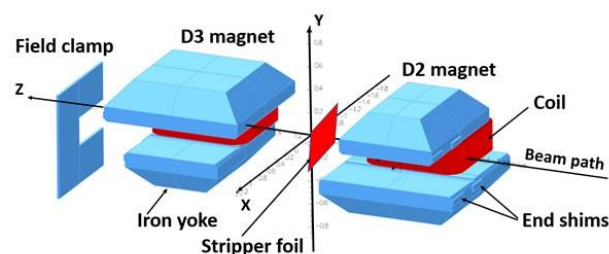

Fig. 1. Chicane magnets.

The peak field in these magnets should be less than 0.25 T (D2) and 0.21 T (D3), respectively, to avoid electron stripping by the magnetic field (see Fig. 2).
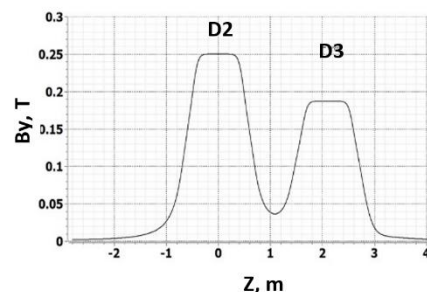

Fig. 2. Vertical field component in D2-D3 magnets. Z = 0 in the D2 magnet center, z=2.1 m for the D3 center. The foil placed at z=0.47 m.

The magnet cross section shown in Fig. 3. The outer magnet gap is 248 mm which is 10 mm smaller than inner gap to compensate a natural in C-magnets field gradient.
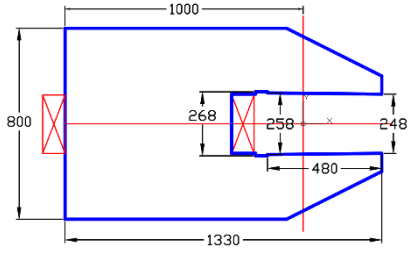
Fig. 3. Chicane magnet cross section. Dimensions in mm.

The stripper foil is mounted downstream of magnet D2. The magnetic field in the foil area must be less than 0.22 T, with the field vector **B** having tilt of arctg(Bz/By) > 0.1 rad. To achieve this, the upper pole of magnet D2 was made 0.4 m shorter than the bottom one. In the old magnets, the magnet D3 had a special configuration to compensate for the deviation from the requirements for the ideal integrated homogeneous field for both magnets. However, because both magnet yokes are not saturated, it was more effective just to use the same geometry for D3 as for D2 but rotated around the x-axis at 180°. This can compensate for most of the field disturbances caused by having different pole lengths. The residual high field harmonics were compensated for by pole end shims, as shown in Fig. 1. These shims have dimensions 51 mm x 200 mm with 15 mm thickness. They made detachable for the final magnetic field tuning after magnetic measurements.

Another difference between the new and old magnets is that the coils were placed around the poles in the old magnets but mounted around the return yoke in the new coils (see Fig. 1). This reduces the pole-end effects, increases the width of good field area, and makes it easier to protect the coils from high radiation [5] losses. This change also allows magnet D2 and D3 to be mechanically identical. D3 is magnet D2 but rotated around the x-axis. The magnets' specifications and parameters are shown in Table 1.

TABLE I
SPECIFICATIONS AND DESIGN PARAMETERS

Parameter	Units	Specification	Design
Gap between pole tips	mm	248	248
Total integrated field	T-m	0.5939	0.608
D2 peak field	T	0.25	0.2503
D3 peak field	T	<0.2	0.1873
Integrated field to foil*	T-m	0.2847	0.2938
Integrated field harmonics at Rref=100 mm	Units**	< 10	< 8
D2 coil ampere-turns	kA		51.308
D3 coil ampere-turns	kA		38.32
D2 pole length upper/bottom	m		0.91/1.31
D3 pole length upper/bottom	m		1.31/0.91
Magnet stored energy/magnet	kJ		37.2
Iron yoke volume/magnet	m^3		1.725
Iron yoke weight/magnet	ton		13.6
Coil number of turns			30
Coil current D2/D3	A		1710/1277
Copper conductor	mm		15.9x38.1
Voltage drop D2/D3	V		6.2/4.6
Power D2/D3	kW		10.6/5.9
Water temperatures rise D2/D3	°C		8.5/4.7

*For x=y=0, z=0.47 m.

** Unit is 10^{-4}.

An integrated magnetic field analysis was performed in two steps. Initially on the basis of 3D magnetic field simulation for both magnets, the integrated field was calculated on the surface of 100 mm cylinder radius placed on the central magnet axis. After that, the harmonic analysis was conducted using obtained integrated field components. Table 2 shows normal and skew integrated harmonics for magnets D2 and D3 at the reference radius of 100 mm. The results meet the harmonics specification of lower than 10 units (10^{-3}).

TABLE II
NORMAL AND SKEW INTEGRATED HARMONICS

Harmonics	Normal	Skew
Dipole	10000	7.8
Quadrupole	3.6	6.6
Sextupole	1.8	-0.6
Octupole	-7.4	-0.3

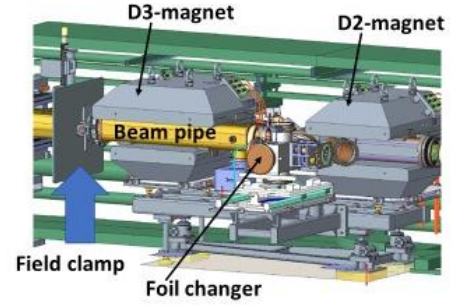Fig. 5 shows the magnet system final mechanical design placed in the tunnel.

Fig. 5. Design of the chicane magnets.

III.   INJECTION SEPTUM MAGNET

The injection septum magnet provides simultaneous bending of 1.3 GeV energy of *H⁻* and *H⁰* (proton) beams, as shown in Fig. 6.
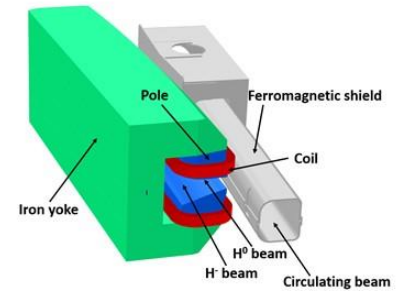

Fig. 6. Model injection septum magnet for the field simulations.

Designing this new magnet involved several issues:
- The magnetic field should have a strong 0.1827 m^{-1} quadrupole term.

- A large 150 mm separation and different bending angles are needed between the H^- and H^0 beams.
- Very low fringe field is needed in the circulating beam area.

The magnet's specifications and parameters are shown in Table 3.

TABLE III
SPECIFICATIONS AND DESIGN PARAMETERS

Parameter	Units	Specs	Design
Gap between pole tips (min)	mm	64	64
Distance between H⁻ and H⁰ beams	mm	150	150
H⁰ bend angle	mrad	181.65	181.42
H⁻ bend angle	mrad	125	125.76
Quadrupole field term	m⁻¹	0.1827	-
Maximum physical length	m	2.2	2.156
Maximum current	A	4700	4583
Coil ampere-turns	A	-	18330
Number of turns/coil			4
Copper conductor	mm		15.9x38.1
Total voltage	V		11.5
Total power	kW		52.7
Water pressure drop	MPa		1.0
Water temperature rise	˚C		18.3

The quadrupole field component in the magnet gap was obtained from the hyperbolic pole tip profile $y = 16928 / x$, where x and y are in mm. This profile has end shims to compensate for the pole end effect and has a minimum 68 mm vertical distance for the beam pipe (see Fig. 7).
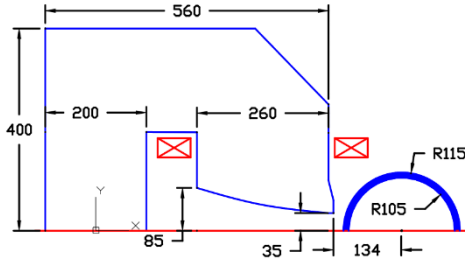

Fig. 7. Septum magnet cross section.

Because the requested field gradient fixes the pole tip profile, there is only one opportunity to fit the requested beam bend angles by the pole end variations. The best variant had 15° chamfers on both pole ends, as shown in Fig. 8. These chamfers provide a shorter effective pole length for the H^- beam than for the H^0 beam.
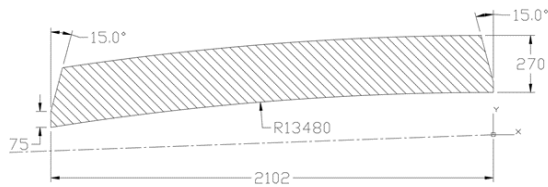

Fig. 8. Top view of the pole tip. Dimensions in mm.

The final magnetic field tuning will be performed after the magnetic measurements, with the help of detachable pole tip end plates. An even more challenging task was minimizing the fringe field in the circulating beam area. In the first variant, the conventional approach for septum magnets was used by placing the coil in the space between the H^0 and circulating beams. However, further analysis showed that there was not enough space for the coil and that this area would have very high losses of coil radiation. The coil was lifted vertically from the magnet's middle plane. This had two drawbacks: the field dropped in the magnet gap under the pole edge, and a larger fringe field was observed in the circulating beam area. The first effect was suppressed by increasing the end shims of the pole tips. The second was reduced through ferromagnetic shielding of 10 mm thick low carbon steel, as shown in Fig. 7. In this case, the fringe field inside the shield was in the range of 5–15 Gauss. Because the circulating beam pipe has in an addition a Mu-metal shield, this value will be further suppressed to an even lower value.

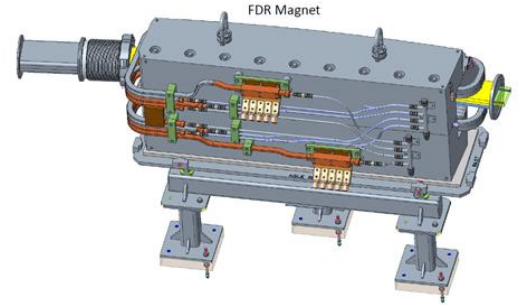The magnet's design is shown in Fig. 9.

Fig. 9. Injection dump septum magnet.

IV. EXTRACTION LAMBERTSON MAGNET

The extracted beam should be bent in the magnet gap without disturbing the circulating beam passing through the upper pole hole. In the old magnet, a large -37 units of skew quadrupole component was observed in the magnet gap, caused mostly by pole field end effects [8]. Magnetic field simulations were performed to propose magnet field improvements for the existing magnet. The simulated magnet model is shown in Fig. 10.
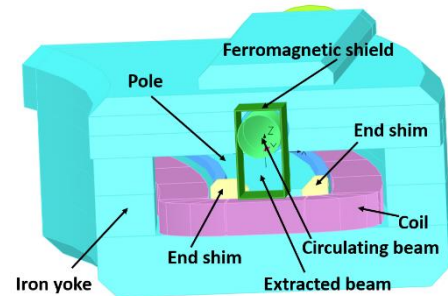

Fig. 10. Model extraction Lambertson magnet.

Variants were investigated with different gaps, far ends, and front pole end shims. The best results were obtained with the front shims shown in Fig. 10. The main reason is that most of the field distortions in this area were caused by the very small

ferromagnetic wall thickness (3.6 mm) between the magnet gap and the pole hole for the circulating beam. Additional shims corrected the magnetic field distortions to lower than 3 units (10^{-4}), as shown in Table 3.

TABLE III
FIELD HARMONICS IN THE MAGNET GAP

Harmonic number	bn*	an*
0	1.0001	$1.8 \cdot 10^{-3}$
1	$-2.8 \cdot 10^{-4}$	$1.1 \cdot 10^{-4}$
2	$3.3 \cdot 10^{-4}$	$2.5 \cdot 10^{-4}$
3	$7.5 \cdot 10^{-5}$	$-1.0 \cdot 10^{-4}$
4	$1.9 \cdot 10^{-4}$	$8.1 \cdot 10^{-6}$
5	$-1.2 \cdot 10^{-5}$	$7.4 \cdot 10^{-5}$

* bn- normal, an- skew harmonics for the reference radius 50 mm.

The magnetic field harmonics were analyzed in several steps. Initially, the 3D magnetic field was simulated, and proton particle-tracking analysis was performed. Afterward, the magnetic field components were integrated along the particle tracks. Then, field harmonics were computed for the integrated fields, as shown in Table 3. The particle-tracking analysis proposed in [8] also gave useful information about beam distortions. The elliptical beam was injected in the front of the magnet, and the coordinates of the particles crossing the plane normal to the tracks were analyzed at the magnet end. The analysis shows how the initial elliptical beam profile changed at the magnet's far end (see Fig. 11).
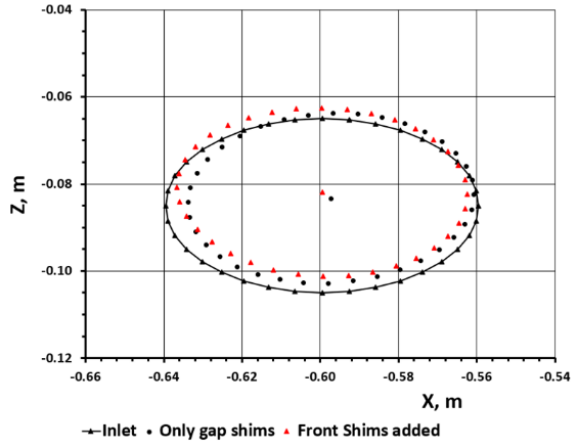

Fig. 11. Beam profile distortions for the variant with only magnet gap shims and with front-end shims added.

In addition, the beam phase space distortions were also extracted, which was 6 mrad with only gap shims and only 1 mrad when end shims were added.

The pole and end shims were made detachable to allow for fine field tuning based on the magnetic measurements and the beam performance in the target area.

The fringe field inside the pole hole should be as low as possible for Lambertson-type magnets. This was achieved by increasing the length of the upper pole relative to the bottom pole at both magnet ends, which partially compensates for the field distortions at the magnet ends.
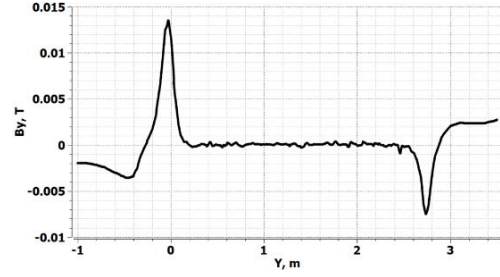

Fig. 12. Fringe field inside the pole hole along the circulating beam path.

Note the rather large field spikes at both pole ends in Fig. 12. Because they have opposite signs, the integrated field is only $0.88 \cdot 10^{-3}$ T-m, which could be easily compensated for by a downstream dipole corrector.

CONCLUSION

The magnet designs of the magnets described above meet the required magnet specifications. Nevertheless, deviations might exist in the iron's magnetic properties, machined parts, and assembly. At Fermilab, the design and fabrication of magnetic field measurement systems have begun, including for the Hall probes, rotational coils, and stretch wire techniques. The measured results will be compared with simulations. Any unacceptable field deviations should be corrected with detachable end shims.

REFERENCES

[1] "Spallation Neutron Source", neutrons.ornl.gov/sns.
[2] S. Henderson, *et. al*., "Status of the SNS Beam Power Upgrade Project", Proc. of EPAC 2006, Edingburgh, Scotland, MOPCH129, 2006.
[3] P. Wanderer, *et. al*., "The SNS Ring Dipole Magnetic Field Quality", Proc. of EPAC 2002, Paris, France, pp. 1317-1319.
[4] P. Wanderer, *et. al*., "Final Test Results for the SNS Ring Dipoles", Proc. of PAC 2003, pp. 2159-2161.
[5] D. T. Abell, Y. Y. Lee, W. Meng, "Injection into the SNS accumulator Ring: Minimizing Uncontrolled Losses and Dumping Stripped Electrons", Proc. of EPAC 2000, Vienna, Austria, pp. 2107-2109.
[6] J. G. Wang, "Magnetic Field Distribution of Injection Chicane Dipoles in Spallation Neutron Source Accumulator Ring", Physical Review Special Topics-Accelerator and Beams 9,012401, 2006.
[7] "Opera Simulation Software", Dassault Systemes UK Ltd 1984-2021.
[8] J. G. Wang, "Performance improvement of an extraction Lambertson septum magnet in the Spallation Neutron Source accumulator ring", Physical Review Special Topics-Accelerator and Beams 12, 042402, 2009.